THE ASTROPHYSICAL JOURNAL, 534:1008–1019, 2000 May 10

DISTRIBUTION OF SUPERGRANULAR SIZES

R. SRIKANTH, JAGDEV SINGH, AND K. P. RAJU
Indian Institute of Astrophysics, Koramangala, Bangalore- 34, Karnataka, India; srik@iiap.ernet.in, kpr@iiap.ernet.in
Received 1999 June 23; accepted 1999 December 7

ABSTRACT

A gradient-based method of tessellation was applied to *SOHO* Dopplergrams and to Ca II K filtergrams in order to study the cellular pattern of the solar surface, in specific the geometric relationship between the tessellation and the chromospheric network/supergranulation. We found that for zero spatial smoothing and low temporal averaging the above data sets yield mean tessellation scales of 8–10 Mm for the *SOHO* Dopplergrams of 2″ pixel resolution and 14–18 Mm for K line filtergrams of 3.″2 pixel resolution. This difference is attributed to the dependence of the tessellation on the resolution of the images. The distribution of the tessellating tiles shows a broad, right-skewed spectrum, tending to greater broadness, symmetry, and larger scales when the image is smoothed. The skewness and kurtosis curves of the distribution of the tiles as a function of the smoothing show local peaks when the mode of the distribution approaches the traditional supergranular scale of 25 Mm. The values of skewness and kurtosis in this limit, 1.1 and 4.6, respectively, are close to the corresponding parameters for supergranular distribution derived independently, implying that supergranulation may be geometrically identified with the tessellation at the corresponding resolution. Time averaging also leads to an increase in length scale when averaged for up to 30 hr. In the case of Dopplergrams the size increases from 9 to 16 Mm and for the K line filtergrams from 18 to 23 Mm. This feature can be attributed to the suppression of short-lived, small-scale features. The effects of both spatial smoothing and temporal averaging can be explained in terms of enhancement of the supergranular signal.

Subject headings: Sun: atmosphere — Sun: chromosphere — Sun: granulation

1. INTRODUCTION

The chromospheric network was first extensively studied and related to the supergranular velocity fields by Leighton and others (Leighton, Noyes, & Simon 1962; Leighton 1964; Simon & Leighton 1964). Since then a number of studies on the morphology, scales, dynamics (see Srikanth, Raju, & Singh 1999 for a partial list of references), and relationship with surface magnetic fields have been made. Length scales have been studied by a number of authors, since Leighton and others reported a value of about 32 Mm. This value was determined by the method of autocorrelation (Rogers 1970; Wang 1988) and also by taking cross sections of the network/supergranulation in various lines. Singh & Bappu (1981) estimated cell areas to be about 23 Mm by outlining peak emissions on enhanced K line spectroheliograms. Interestingly, they also quoted an autocorrelation (AC) scale of 32 Mm in agreement with Leighton and others. This discrepancy has been attributed to the presence of open cells, which spuriously boost the AC scale (Singh & Bappu 1981), to the particular geometry of the cell shapes (Hagenaar, Schrijver, & Title 1997, and to the inclusion of the intercell spacing in the AC method. Münzer et al. (1989) derived a size of about 28 Mm from a Fourier analysis of the K line network. Raghavan (1983) reports a comparable size measured using quantitative stereology. A partial list of length scales reported by various authors for supergranulation has been compiled in Table 1.

Recently, techniques for the automatic extraction of network structure on the solar surface and study of their geometric properties using computer algorithms have been used. A method of "skeletonizing" the image starting from a binary image based on a threshold value has been used to study the morphological properties such as orientation, elongation, size, fractal dimension, and the temporal variation of the cells as derived by this method (Berilli, Florio, & Ermolli 1998; Berilli et al. 1999). Using a tessellation that employs a gradient-based algorithm, Schrijver, Hagenaar, & Title (1997) studied the patterns of solar granulation and supergranulation, and Hagenaar et al. (1997a) deduced from Ca II K filtergrams a mean cell size in the range 13–18 Mm, which is almost one-half the traditionally quoted value. This method of tessellation is a pattern recognition algorithm for identifying "basins" in the intensity landscape of the image. In this work we have extended the application of tessellation to high-resolution K line images and Dopplergrams obtained from *SOHO* (Scherrer et al. 1995). The aim was to study the behavior of the scales of the tessellating tiles and to draw inferences regarding the geometrical connection between the tiles and supergranular cells.

Knowledge of the length scale and topology of the network coupled with its time evolution is useful for modeling the diffusion process driving the dynamic evolution of the network (Leighton 1964), for example, in estimating the diffusion constant for flux dispersal (Schrijver et al. 1997). Understanding the behavior of surface magnetic fields can shed light on magnetoconvective processes in general.

2. DATA AND PREPROCESSING OF DATA

Two sets of data were used in this study: (1) *SOHO* full-disk solar Dopplergrams (Scherrer et al. 1995) and (2) a time series of Ca II K line data at medium resolution from Antarctica (Singh et al. 1994). Data set (1), from the *Solar and Heliospheric Observatory* (*SOHO*), consists of a time series of Dopplergrams made from five pairs of lines centered around N II λ6768 spaced at 1 minute. The part of the data set used by us covers a period of 32 hr. The pixel resolution is about 2″ pixel^{-1}, which implies spatial resolution of 4″. The basic image shows a hazy supergranular signal superposed by prominent noisy small-scale features due to *p*-

TABLE 1

LENGTH SCALE ESTIMATES OF SUPERGRANULES

Investigator	Size (Mm)	Method Used
Hart (1956)	26	AC: Hα Dopplergram
Simon & Leighton (1964)	32.5	AC: various chromospheric and photospheric lines
Simon & Leighton (1964)	25	Microphotometer tracing
Janssens (1970)	28	Visual inspection: Hα
Duvall (1980)	30	AC: Fe I λ8688
Giovanelli (1980)	~30	AC: Fe I λ8688
Sýkora (1970)	32–37	K filtergram AC
Singh & Bappu (1981)	32	AC: K spectroheliograms
Singh & Bappu (1981)	23	Grid counting: K line
Brune & Wöhl (1982)	22–31	Visual inspection: Ca K
Hagenaar et al. (1997)	13–17	Tessellation via steepest descent algorithm
Raju et al. (1998)	30–35	AC: Ca II K
Berilli et al. (1998)	24	Tessellation via binary imaging

modes. In order to remove the effect of low-period oscillations, the Dopplergrams were block averaged over 10 minutes. Visual inspection of these images shows a strong supergranular pattern with the expected distribution property: bright-dark clusters clearly visible in the middle heliographic angles and elongated toward the limb but almost absent from the disk center. Data set (2) is a time series of Ca K line filtergrams covering an uninterrupted duration of 106 hr obtained in the Antarctic region during the local summer of 1989/1990. The study is based on the quiet region surrounding the spotgroup NOAA/USAF 5784 (central meridian passage 1990 January 10). Details of the preprocessing of the filtergrams involved are given in Raju, Srikanth, & Singh (1998). The digitized, processed images are of medium resolution with a pixel resolution of $3\farcs2$ pixel^{-1}.

3. METHODOLOGY

A method of tessellation based on a two-dimensional basin-finding algorithm (Hagenaar et al. 1997) has been applied to *SOHO* Dopplergrams and comparatively to the K line filtergrams. The method consists of minimizing the intensity/velocity map using the Steepest Descent algorithm to find the local minima. As a second step, all image points are clustered into tiles depending on the local minima on which they converge according to the Steepest Descent algorithm. This ensures that the entire image is covered by nonoverlapping tiles, which by definition constitutes a tessellation. To use a physical analogy, the algorithm may be thought of as recognizing and extracting patterns of "valleys" or "basins" surrounded by "mountain ranges" from the image landscape. K line intensity maps can be studied by this method because of the bright network structure they have. Dopplergrams also show a local mountain-valley structure that can be probed by the tessellation (as well as AC) method. Tiles formed by Dopplergrams have their lowest redshift not at the central upflow region of the underlying supergranule but in the flow directed away from the line of sight. As the flow surrounding the minimum varies continuously in other directions, the redshift pattern forms a well-defined basin.

An example of a tessellation superposed on a K line filtergram window is given in Figure 1. The window size is 125×125 Mm^2, which is expected to contain about 25 supergranules of traditional size. Its tessellation yields about four times as many tessellating tiles. The image is given in the upper panel. The lower panel contains the same image with its tessellation at zero smoothing superposed. The tessellation is seen to divide the window into various tiles. The brighter regions in the top panel usually find a corresponding tile boundary in the bottom panel. However, the converse is not true: some of the tile boundaries are seen to cut through the cells. In such cases, close inspection and sometimes altered image contrast are needed in order to discern the underlying weak intensity rise sensed by the tile boundary. In the right and especially lower right parts of the images in Figure 1 we find a fairly well-defined network pattern. The tessellation also shows a fairly expectable track. The present algorithm, being a tessellation, forces the image into a surface-filling network system of nonoverlapping tiles. As a result, even regions manifesting weak cellular structure, such as the top left part of the image, where the intensity contrast is low and the open cell pattern is reminiscent of formative or dying cells, give rise to a well-defined tessellation.

For studying temporal behavior of the Dopplergram tessellation, we typically used windows of size $140'' \times 140''$. In each successive frame the window has to be shifted in the direction of solar rotation to prevent misalignment. At the center of the disk, the pixel scale is 1.44 Mm pixel^{-1}. Since the solar surficial rotation speed is about 2 km s^{-1}, we can estimate that every 12 minutes, the window should be shifted by 1 pixel. As the images had been time averaged over 10 minutes, this means shifting the window by 5 pixels per six frames. For regions at higher heliographic latitude and longitude, the ratio decreases because of projection effects both on the size and rotation speed. In practice, we additionally ensured registration of the images in the time series by supplementing the main computation program with a subroutine to align the images with respect to the initial window by means of maximizing the cross-correlation function.

4. SPATIAL SMOOTHING AND TESSELLATION

In Figure 2, a tessellation of an unsmoothed *SOHO* Dopplergram window of size 140×140 Mm is given. The average size (defined as the square root of area) of the tiles is about 10.5 Mm and the maximum size about 19.5 Mm. Tessellation of the images in Ca II K yields an average and maximum tile size of 14 and 26 Mm, respectively. Here we note the result of Hagenaar et al. (1997), who quote a range of 13–18 Mm for the tessellation scale of K line filtergrams

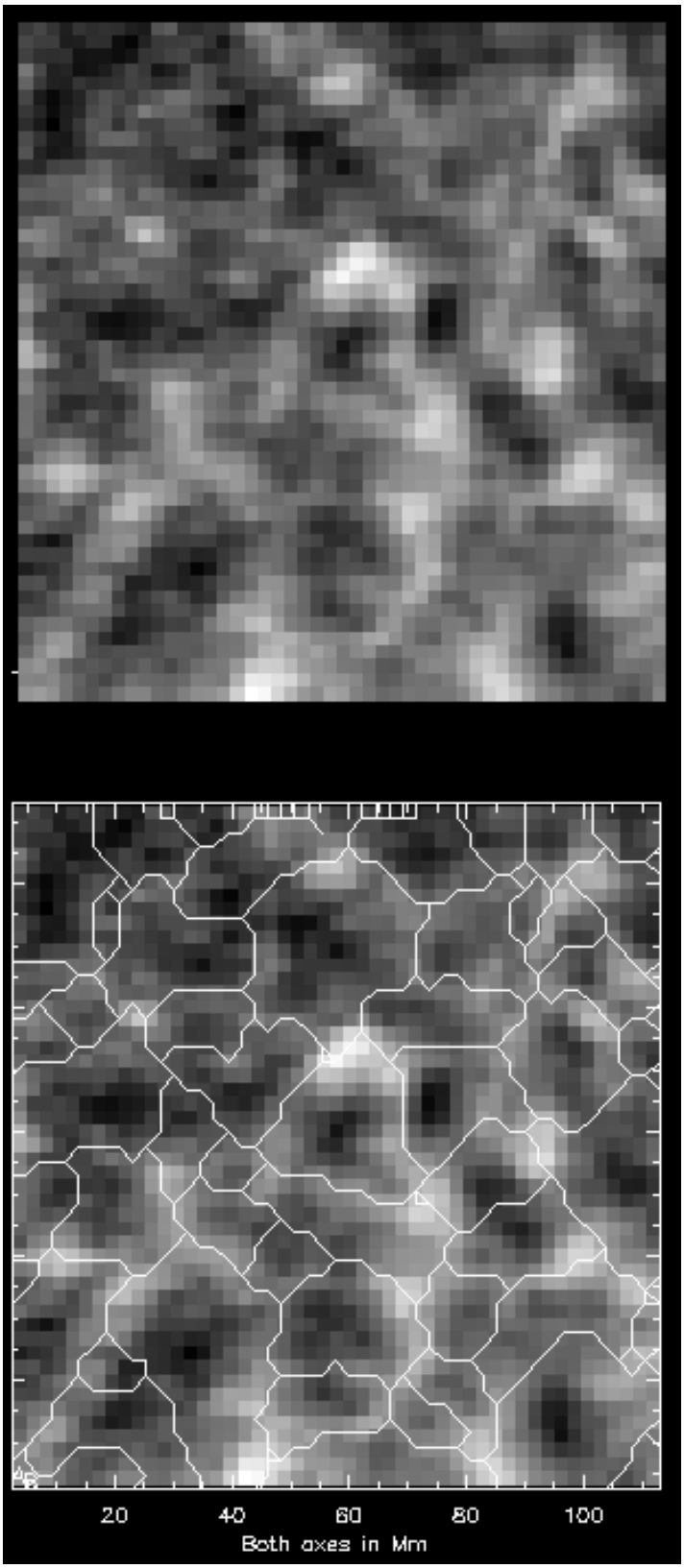

FIG. 1.—Tessellation of a 125 × 125 Mm^2 region on a K line filtergram. *Top:* Image window. *Bottom:* Window upon which is superposed the corresponding tessellation. The mean size (square root of area) of the tiles is 14.7 Mm.

of similar resolution. From our data we find that both the mean and maximum tile size of the K line filtergram tessellation are about 1.4 times larger than the corresponding Dopplergram scales. Hagenaar et al. (1997) identify the tessellation of medium-resolution K line intensity maps with supergranulation. Analogously, in view of the closeness of the Dopplergram tessellation scale to mesogranular scales, one might consider a possible connection between Dopp-

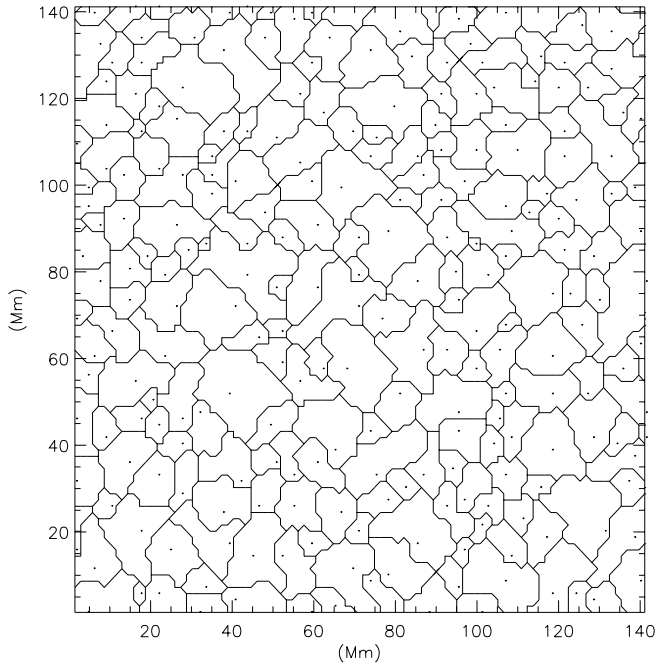

FIG. 2.—Tessellation of a Dopplergram on a window about 140″ × 140″ in size. Intensity minima for each tile (*dots*) are shown.

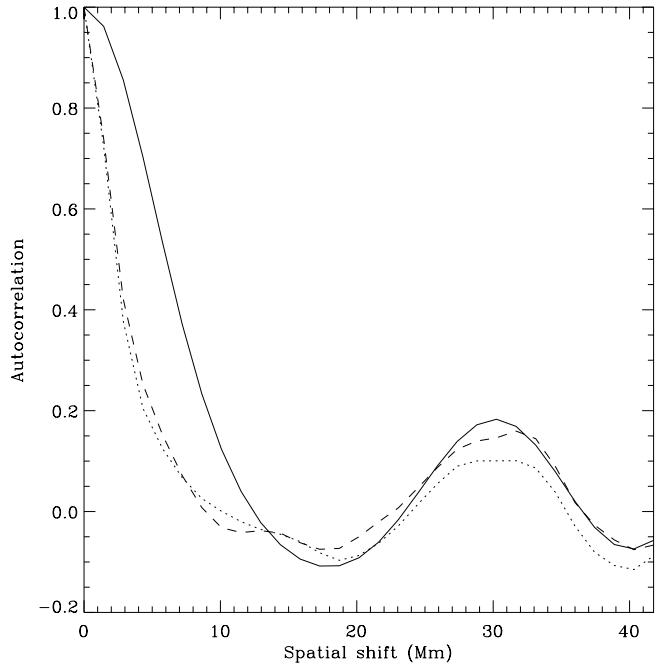

FIG. 3.—AC curve for a 140″ × 140″ window for a single exposure (*dotted line*) and the same image smoothed by convolution with a Gaussian of FWHM = 4″ (*solid line*) and time averaged over 10 minutes (*dashed line*). Both spatial smoothing and time averaging tend to remove noise and hence enhance the supergranular signal.

lergram tiles and mesogranules. Hagenaar et al. further note that the tile pattern can be closely modeled as a Voronoi tessellation, with the seed points being associated with upflow centers in supergranules.

Apart from supergranules, the input images contain signals that could arise from short-term modes, mesogranulation, and other short-lived small-scale phenomena. The relative contribution of these features is modified by spatially smoothing and/or temporally averaging the raw images. In Figure 3, the AC functions of a 140″ × 140″ Dopplergram window are given. The dotted line represents AC of a raw *SOHO* Dopplergram. The dashed line stands for AC of the window time averaged over 10 minutes and the heavy line for the same window spatially smoothed by convolution with a Gaussian of FWHM = 4″. All three give an AC size of about 30 Mm in agreement with traditional results, demonstrating the stability of correlation length scale with respect to smoothing of the image. In the next three sections, we shall consider the effect of smoothing on the size, distribution, and shape of the tessellating tiles.

4.1. *Scales*

Smoothing of the image causes intensity contrasts to be leveled out by redistributing intensity from higher to lower intensity regions. As a result, it causes tile boundaries of sufficiently low intensity contrast to vanish, leading to merger of tiles and consequent increase of the mean size of tiles. This is depicted in Figure 4, where the four inlaid figures are tessellations of the same window smoothed with $\lambda = 0$, 1, 2, and 4 Mm, where λ is the FWHM of the Gaussian with which the image is convolved to smooth it. Here we find evidence for smaller tiles combining to form larger ones, though this can also be accompanied by shape changes of the tiles. Data for the dependence of the tessellation scale on λ in both *SOHO*/Michelson Doppler Imager (MDI) Dopplergrams and K line filtergrams are given in Figure 5. The heavy curve (representing Ca II K) has a tessellation scale of 14.5 Mm at zero smoothing, about 5 Mm more than that of Dopplergrams, represented by the dashed line. However, at higher λ, both curves tend to converge. The dependence of tessellation scale on λ is in contrast to AC scale, which, as noted in connection with Figure 3, is fairly stable.

The initial separation and later convergence of the curves can be attributed to the different resolutions in the K line filtergrams and Dopplergrams. From the formula

$$(\text{effective resolution})^2 = (\text{resolution})^2 + \lambda^2 \qquad (1)$$

we can relate the effective resolution of the smoothed image to the resolution of the original image and the smoothing parameter λ. The respective pixel resolutions in the Dopplergrams and the K line filtergrams are 2″ and 3.″2. According to equation (1), for $\lambda = 2.''5$ the effective resolution of the Dopplergrams equals the resolution of the filtergrams. From Figure 5 we find that the tessellation scale for Dopplergrams at $\lambda = 2.''5$ is about 14.5 Mm, which is close to the tessellation scale for the filtergrams at zero smoothing. Furthermore, equation (1) implies that for sufficiently large λ, the effective resolutions in the filtergrams and Dopplergrams are close. This is consistent with the observed tendency for both the curves in Figure 5 to converge. This dependence of tessellation scale on resolution and λ underscores a necessity to exercise caution in applying this method to study scales. Identifying supergranulation (or mesogranulation) with the tessellation will make the size of supergranules (or mesogranules) resolution dependent. To avoid this, we must select a criterion that somehow singles out the resolution that corresponds to supergranulation, a point that becomes clearer in the next subsection.

4.2. *The Distribution Function*

The distribution of tile sizes obtained from the tessellation of Dopplergrams shows a broad asymmetric pattern

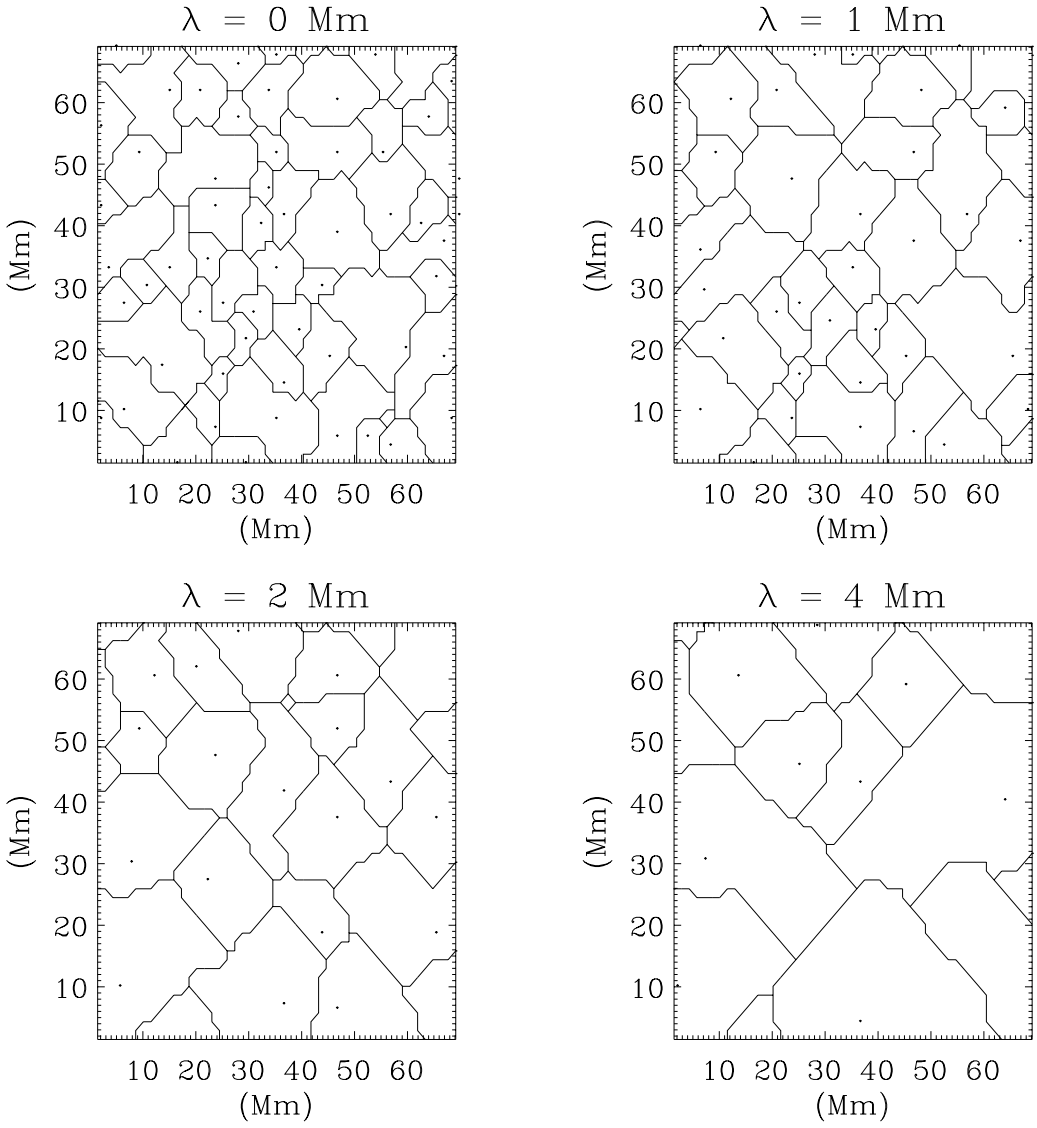

FIG. 4.—Tessellation of the same 140″ × 140″ *SOHO* Dopplergram window smoothed with $\lambda = 0.0$, 1.0, 2.0, and 4.0 Mm

skewed to the right-hand side similar to that obtained from a tessellation of K line filtergrams (Hagenaar et al. 1997) and also distributions of cell scales obtained according to conventional methods (Simon & Leighton 1964; Singh & Bappu 1981; Singh et al. 1994; Srikanth et al. 1999). Both the asymmetry and the peakedness of the distribution is larger for a histogram of areas than for one of length scales because of the way a distribution transforms under a transformation of the random variable (Srikanth et al. 1999). Interestingly, Berilli et al. (1998), using a different method of tessellation, report that the distribution of cells rises monotonously toward smaller cells, reminiscent of the distribution of granular sizes reported by Muller & Roudier (1994). Because of the simplicity of the distribution function (e.g., no double peaks), we can quantitatively characterize the shape of the distribution in terms of its skewness and kurtosis (Srikanth et al. 1999a). For a data set $\{x_i\}$ of n points, where standard deviation is given by

$$\sigma \equiv \left[\frac{1}{n}\sum_{i=0}^{n}\{(x_i - \bar{x})^2\}\right]^{1/2}, \tag{2}$$

skewness is given by

$$\alpha \equiv \frac{1}{n\sigma^3}\sum_{i=0}^{n}\{(x_i - \bar{x})^3\}, \tag{3}$$

and kurtosis is given by

$$\beta \equiv \frac{1}{n\sigma^4}\sum_{i=0}^{n}\{(x_i - \bar{x})^4\}. \tag{4}$$

Skewness and kurtosis measure, respectively, the asymmetry and peakedness of a distribution about its mean. The definition of either parameter ensures that it depends only on the shape and not a scale factor of the distribution.

Skewness and kurtosis were calculated as a function of number n of tessellating tiles. Above a sufficiently large n the parameters stabilize, generally simultaneously. In Figure 6, kurtosis is plotted for unsmoothed Dopplergrams as a function of number of tiles. The function is more or less constant for $n > 3500$. The values of the parameters are calculated as the mean value in this stable regime. Mean and standard deviation in this range give a value $\beta = 6.63 \pm 0.09$. Simi-

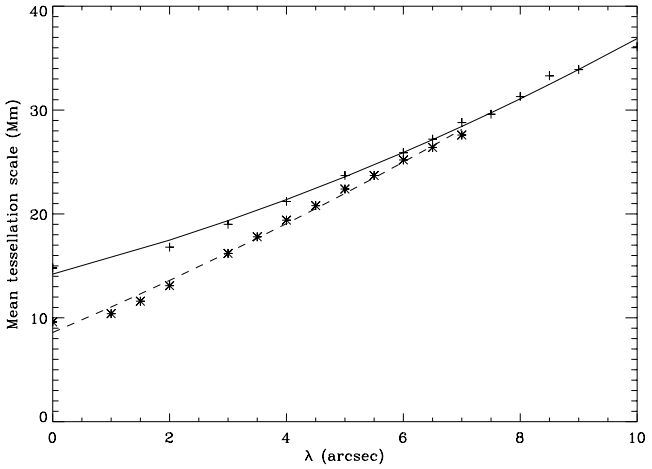

FIG. 5.—Average size of tiles as a function of λ. Mean tile sizes for K line filtergrams (*plus signs*) with a second-order best fit (*heavy line*) and mean tile sizes for the *SOHO*/MDI Dopplergrams (*asterisks*) with a second-order best fit (*dashed line*) are shown. The tessellation scales for the two data sets at zero spatial smoothing are, respectively, about 14.5 and 8.6 Mm. Both data points converge for large smoothing.

larly, we find for skewness $\alpha = 1.65 \pm 0.01$. It turns out that the minimum image area required for skewness and kurtosis functions to stabilize is a constant, about 3×10^4 Mm^2, irrespective of λ. Consequently, the number of tiles n at which α and β stabilize is smaller for larger values of λ. Hagenaar et al. (1997) found that the distribution of the tiles remains self-similar under smoothing (α, β = const), but we noted an overall tendency toward a more nearly Gaussian shape. The values of α and β at different length scales are given in Figure 7, wherein λ has been reparameterized to length scale according to the Dopplergram curve in Figure 5. We note the fairly low error bars. Both skewness and kurtosis show a similar trend. Except for local peaks near 11 and 26 Mm, the main trend is one of falling value of skewness and kurtosis as mean scale increases, meaning that the distribution becomes less asymmetric and less peaked for larger λ.

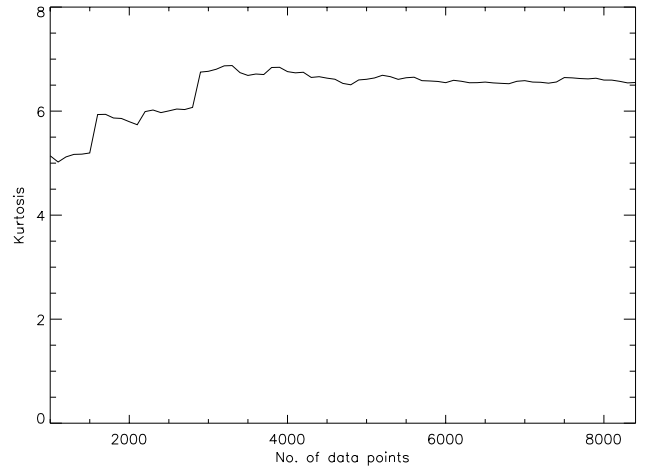

FIG. 6.—Plot of kurtosis of a region from an unsmoothed Dopplergram as a function of number of data points. As the number exceeds some threshold value (corresponding to a tessellated area of $\sim 3 \times 10^4$ Mm^2), the value of kurtosis stabilizes. The mean value of kurtosis in this regime is considered as the characteristic value for the distribution of tiles.

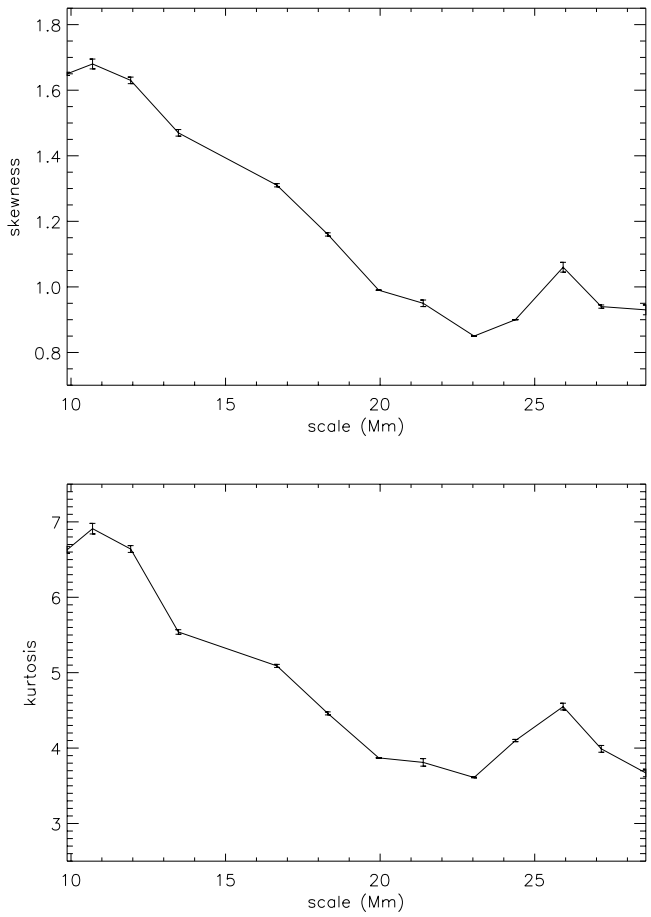

FIG. 7.—Skewness and kurtosis of the distribution of the tessellating tiles as a function of the mean scale (parameterized by λ) of the Dopplergrams. The overall pattern is a fall except for upward kinks near sizes 11 and 25.9 Mm.

A visual appreciation of this trend can be obtained by inspecting Figure 8. Here the distributions of the tiles for four distinct values of λ in increasing order are given. In each case, the length scale in the abscissa is factored so that the mean scale equals 1.0. Frequency is renormalized so that the area under the histogram equals unity, in order to see purely the shape changes in the distribution function. It is apparent that as λ increases (from Fig. 8*a* to 8*d*), tiles are depleted at smaller scales and added toward larger scales. As a result, the amplitude of the peak becomes lower and the peak shifts rightward to a less asymmetric position. This can be explained if we make the reasonable assumption that smaller tiles correspond to more shallow basins on the velocity landscape of the Dopplergrams and larger tiles to deeper basins. Thus, the chances of two smaller tiles combining under a smoothing operation are greater than those for larger tiles. Since the distribution is concentrated in smaller tiles in the unsmoothed image, the distribution becomes less skewed and less peaked as the image is smoothed.

However, an interesting observation that emerges from Figure 7 is that the overall fall of α and β with scale is not monotonous. At two points the distribution departs from the trend toward a Gaussian distribution. This is at the scales 10.7 and 25.9 Mm, where local peaks are seen, more so in the latter point. At and about these two points, the

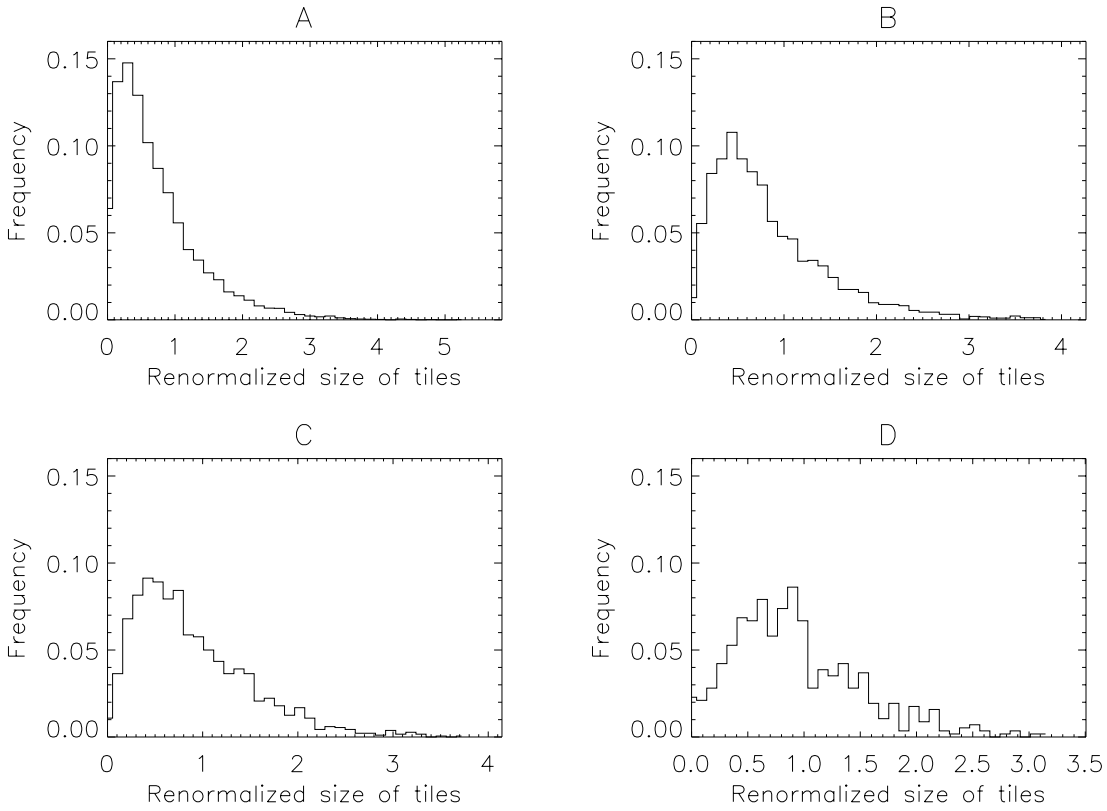

FIG. 8.—Renormalized distribution of tiles derived from Dopplergram tessellation with (*a*) $\lambda = 0$ Mm, (*b*) $\lambda = 1.6$ Mm, (*c*) $\lambda = 2.8$ Mm, and (*d*) $\lambda = 5$ Mm. In the independent axis, mean tile sizes are rescaled to equal 1. The more the image is smoothed, the less asymmetric and less peaked the distribution is seen to become.

distribution becomes more asymmetric and peaked, significantly larger than the error bars. This can be explained by the existence of intrinsic (i.e., resolution- and smoothing-independent) scales in the Dopplergrams. When the mode of the tile size distribution equals an intrinsic scale, a good many tiles will tend to coincide with the physical structures responsible for the intrinsic scale. We can visualize that when the image is suitably smoothed (6″.5 for Dopplergrams), the boundaries of most of the tiles coincide with those of cells with deeper basins as seen in the intensity patterns.

We note that the two peaks occur, respectively, close to the mesogranular and traditional supergranular scales. To test that the intrinsic structures responsible for the second peak are supergranules, we compared the distributional properties of supergranules (obtained independently) with those of the tiles at 25.9 Mm scale. In Srikanth et al. (1999), the values for skewness and kurtosis, derived from a statistical study of supergranular sizes according to the AC method, are quoted to be 1.1 and 4.9, respectively. This is in agreement with the values $\alpha = 1.06 \pm 0.03$ and $\beta = 4.55 \pm 0.09$ at the 25.9 Mm peak. Here we assume that AC scales are linearly related to true scales of supergranules. This ensures that the distributional property of supergranules is not affected by the use of the AC method. Hence, we associate the second peak in Figure 7 with supergranular scale. By analogy, the first peak, at 10.7 Mm, could be associated with mesogranulation. The corresponding distributional parameters are $\alpha = 1.68 \pm 0.03$ and $\beta = 6.91 \pm 0.14$. The skewness is close to that of supergranules, but the distribution is more peaked. Verification of this by an independent study of mesogranulational size distribution would further corroborate the usefulness of the tessellation method to study scales. The mode of the distribution at the 25.9 Mm peak was found to be 25 Mm, which is estimated to be the size of supergranules, in agreement with the scale found by Singh & Bappu (1981) and Küveler (1983), and with that of Berilli et al. (1998) for the critical area ($\equiv$24 Mm) at which the geometrical properties of cells are reported to change. A preliminary study in this respect of K line filtergrams strengthens this result, with an intrinsic size emerging at a mean tile size of 25.9 Mm, which is associated with supergranules. This value is closer to supergranular sizes determined by visual inspection (Simon & Leighton 1964; Janssens 1970; Singh & Bappu 1981), rather than to AC sizes.

4.3. *Circularity of the Tiles*

The shape of a tile may be quantified by the fractal dimension of its perimeter, which can be derived statistically from the slope of the log (area) versus log (perimeter) plot (Muller & Roudier 1994). For our purposes, we found it sufficient to use a parameter "circularity," which can be defined even for a single cell on a flat two-dimensional plane. Defined

$$\kappa = \frac{4\pi \times \text{area}}{(\text{perimeter})^2}, \tag{5}$$

it is a measure of how closely a tile resembles a circle. κ takes values in the range $0 < \kappa \leq 1.0$. On a flat surface, it takes the value 1.0 for circles and smaller values for other

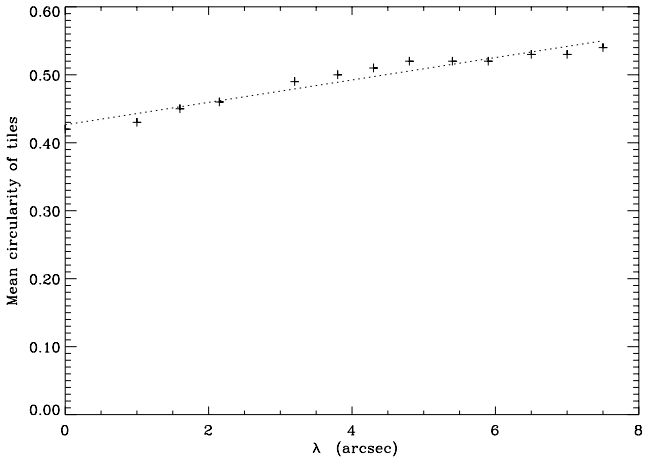

FIG. 9.—Circularity parameter for K line filtergrams as a function of λ

shapes. For example, $\kappa = 0.785$ and 0.698 for a square and a regular hexagon, respectively. A corrugation of the walls of the tile reduces κ since it increases the perimeter without considerably adding to the area.

A plot of the mean circularity of the tiles against λ for the Dopplergram data is given in Figure 9. Typically the circularity of tiles is in the range 0.4–0.5. That means the tiles are typically more irregularly shaped than a regular hexagon. Either a mildly rising trend, such as that depicted in Figure 9, or a lack of dependence on spatial smoothing is observed. The filtergram tessellation also shows a similar behavior.

5. TIME AVERAGING AND TESSELLATION

Time-averaging behavior of the tessellation was studied by averaging cospatial windows and tessellating them. A typical dependence of the tessellation scale on time averaging is given in Figure 10. The x-axis gives the time duration over which cospatial windows have been averaged. The upper curve (marked with plus signs) represents the mean tessellation size for filtergrams, and the lower curve (marked with crosses) represents that for Dopplergrams. In both cases, tile size rises at first relatively rapidly, then slows down and appears to level out beyond 25 hr. The Dopplergrams show a rise from about 9 to 16 Mm. The K line data show a rise from 17.5 Mm to slightly over 23 Mm. The null dependence on time averaging reported by Hagenaar et al. (1997) seems to be confined in our study only to large time intervals (>25 hr).

The behavior of scale in Figure 10 can be explained by the enhancement of the signal due to long-timescale structures by the averaging out of short-timescale processes. Thus, it might be expected that time averaging will increase the tessellation scale. This accounts for the rise in scale in Figure 10. Another factor affecting the time-averaged tessellation is that newer patterns emerge with time. Therefore, for large time, the average image pattern will become randomized because of superposition of uncorrelated structures. As a result, existing boundaries will be crisscrossed by new ones. This is expected to lead to a reduction in tessellation scale. We confirmed this by finding the tessellation scale for images obtained by averaging unrelated (i.e., noncospatial) windows. The result is given in Figure 11. However, we note that the change in tessellation scale is much smaller than one would have expected on the basis of the unrelatedness of the images.

The undulations in the curves in Figure 10 are worth noting. For example, the deviation from the best fit around time $t = 15$ hr is as high as 14% in both the Dopplergram and filtergram curves. Since the number of frames for time $t > 20$ hr is at least 120 frames, and hence contribution of noise will be low, we believe that the undulations in scale are not artifacts. Whether these are indeed related to the undulations in the correlation function noted by Raju et al. (1998) will be investigated elsewhere.

The circularity of the tiles as a function of time averaging for Dopplergrams is plotted in Figure 12. The initial small rise and later fall is not typical for all windows. However, we generally found both in Dopplergrams and filtergrams that the plots have a relatively narrow spread and are confined

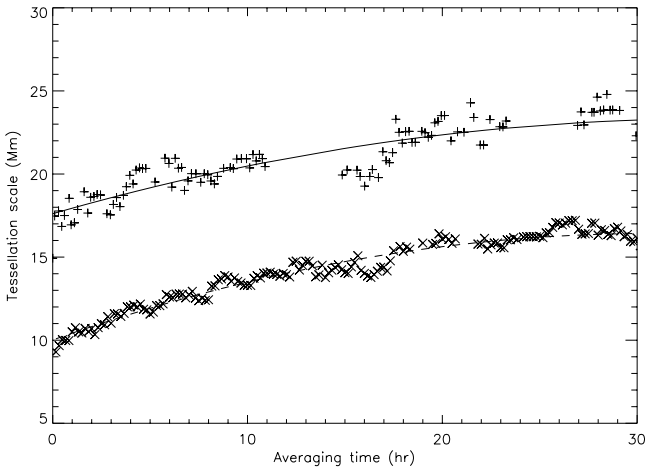

FIG. 10.—Tessellation scale as a function of time duration over which images are averaged. The upper data points and fit curve represent data from filtergram tessellation; the lower ones represent Dopplergram tessellation. Both show an initial rising trend from values of, respectively, about 17 and 9 Mm.

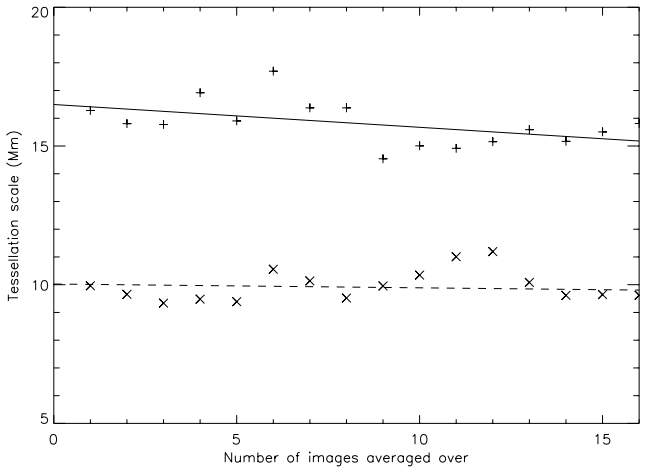

FIG. 11.—Length scale derived from tessellation of the average of various numbers of unrelated windows of equal size. The upper data points and heavy straight-line fit curve represent filtergram tessellation. The lower data points and dashed straight-line fit represent *SOHO*/MDI Dopplergram tessellation. The randomization of features due to the averaging of arbitrary images is expected to produce a rapid fall in the tessellation scale. However, both fits show a gentle fall.

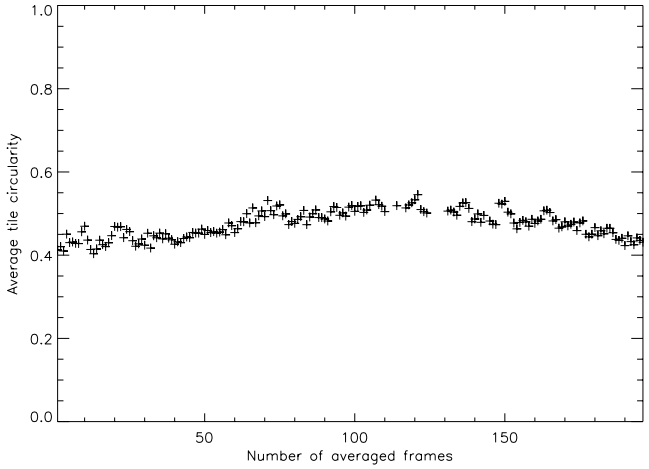

FIG. 12.—Mean circularity of the tessellating tiles as a function of time duration over which images are averaged in a 140″ × 140″ window. We do not find any interesting common trend for this variable among different windows. The rise-fall pattern found in the figure is specific to this window.

to a band in the 0.4–0.5 region. An undulatory character is seen in these plots also.

6. DISCUSSION

6.1. *Physical Significance of Tessellation*

In the first step of minimizing a two-dimensional function, the basin-finding algorithm recognizes only local minima that lie inside spatial undulations resolvable in the given image. For example, if in an image small-scale basins are superposed on a larger basin containing the global minimum, then the tessellation will pick out minima within the smaller basins. In this sense, it tends "not to see the forest for the trees." Its effectiveness as a supergranule-identifying method rests on the assumption that supergranules as basins exist in a one-to-one relation with the local minima occurring in the image.

However, it is obvious from experience that, in the kind of image sets that have been tessellated, local minima occur at smaller scales than supergranules. For example, mesogranules are reported to be about 10″ in size (Oda 1984). As they occur at a smaller scale (and hence more densely), they may interfere with the tessellation pattern. In the case of Dopplergrams, scales associated with coherence length of residual *p*-modes in the filtered images are also possible candidates for forming tiles (though their contribution will be minimal because of the filtering). Another source of inordinately small tiles is open cell regions, which includes formative and dying cells as well as intercellular space. By design, the basin-finding algorithm is a tessellation; i.e., it covers the tessellated region wholly by a system of nonoverlapping tiles. Visual inspection shows that open cell regions have considerable small-scale intensity variations. These are forced into small tiles, further bringing down the mean tile size.

There are also other small-scale candidates that can by definition form tiles at subsupergranular scale: random background spatial fluctuations. Such fluctuations are not of any characteristic scale but occur in a complicated image such as a Dopplergram for a variety of reasons: discontinuities on the cell boundaries, detached cell wall elements from decayed cells, intracell bright points, etc. Fluctuations arising from these will be of a statistical nature and not vary considerably from region to region. In order to test whether tessellation picks up signals from such statistical fluctuations, we studied the tessellation of both Dopplergram and filtergram windows processed as follows. In each case, the window is averaged with itself after the introduction of relative phase shifts with respect to itself. The results of the phase-shifted self-averaging for a typical 224″ × 224″ unsmoothed Dopplergram window are given in Figure 13. The *x*-axis gives the shift in units of AC scale (25.3 Mm for this window) through which the window is shifted to be averaged with itself. At each averaging, the window area is kept constant by including area adjacent to the original window in a continuous way. The *y*-axis gives the AC scales (*heavy curve*) and tessellation scales (*dotted curve*) derived from each self-averaged image in the original AC scale units. The self-averaged image's AC size is seen to vary systematically with the shift. Initially, at zero phase shift, the AC function yields a scale 25.3 Mm. From Figure 13, we see that the self-averaged AC scale remains the same for shifts that are small compared to the cell boundary thickness, which is estimated to be about 5.7 Mm (Singh & Bappu 1981). Thereafter, the phase-shifted self-averaged AC scale rises steeply with increasing phase shift to a value about twice the AC scale. Finally, as the shift approaches one-half the AC scale, the phase-shifted self-averaged AC scale also becomes one-half the AC scale. On the other hand, the tessellation length scale remains almost the same, about 15 Mm for filtergrams, for self-averaged images at varying phase shift. A similar behavior was noted in the case of Dopplergrams, as well.

The behavior of the AC scale reflects the phase difference between intrinsic features in the window between its original and shifted positions. We found that generally the self-averaged AC scale is halved when the shift equals one-half the original AC scale. The reason for this is apparent from the simplified scenario presented in Figure 14. An idealized image profile, with cells separated equally by one actual (i.e., involving no image self-averaging) AC scale unit, is presented in the upper panel. The lower panel represents the image self-averaged at a shift of one-half AC scale. Here the cell

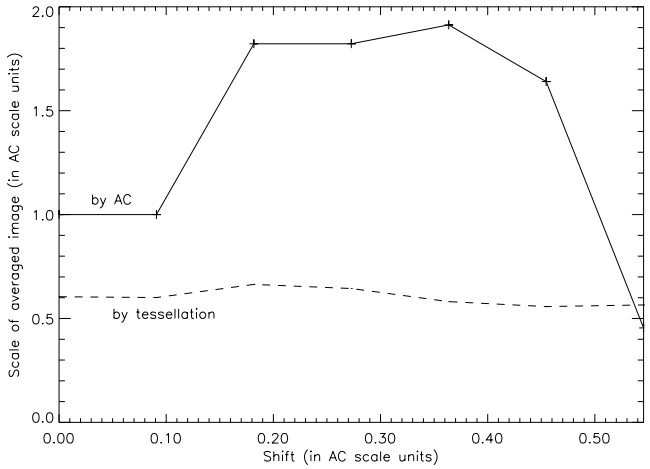

FIG. 13.—Plot of AC and tessellation scale for shifts at which a 224″ × 224″ quiet window is averaged with itself. The scales and shifts are in units of the actual (i.e., involving no image self-averaging) AC scale (25.3 Mm here). The self-averaged image AC scale shows strong variations including a halving when the shift equals one-half the AC size. Tessellation scale is almost constant.

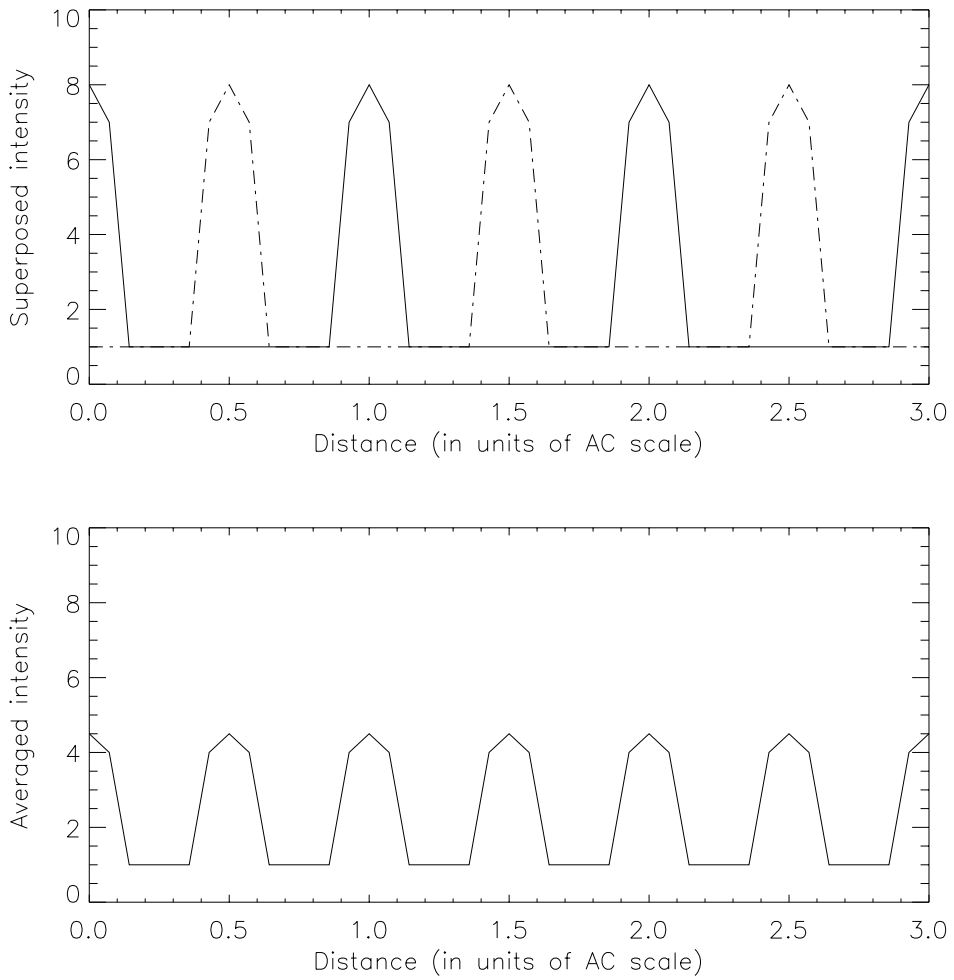

FIG. 14.—Result of averaging an (ideal) window with itself after a shift through one-half an AC scale. *Top:* Profile of boundaries of equal-spaced cells (*heavy line*) and the same profile shifted by one-half an AC scale (*dash-dotted outline*). *Bottom:* Self-averaged profile, with AC length one-half the true value.

walls appear twice as frequently, implying a halving of the AC scale because the cell is split into two in the phase-shifted self-averaged image. The self-averaged AC sizes for other shifts are explained by using a more complicated profile, having unequally spaced cell boundaries of unequal heights. The self-averaged AC scale can exceed the basic AC size because at certain shifts the relative displacements between the cell boundaries in the self-averaged images are interpreted by the AC function as a broadening of the cell wall, which leads to an apparent enlargement of the cell size. On the other hand, the independence of tessellation scale of shift, specifically the fact that it does not halve for a shift of one-half the tessellation scale, means that tessellation reflects intensity variations that may not correspond wholly to intrinsic physical features but to background spatial variations that remain statistically the same at all shifts. We conclude that, for unsmoothed images, the tessellation is independent of actual physical features of interest, unlike the AC function, which shows a strong dependence on the phase of shift in the self-averaged images.

6.2. *Resolution Dependence of Tessellation*

Closely related to the local minimization property of the tessellation is the image resolution dependence of the mean tile size, as seen in Figure 5. Lower resolution means that the smallest "valleys" sensed by algorithm will be larger (and usually deeper) than if the resolution had been higher. Hence, tessellation scales are, as noted, larger for lower resolution. Smoothing of the image reduces the effective resolution of the image and leads to an increase in the mean tile size. The resolution dependence introduces an arbitrariness in the size of the structures defined by the method. It would make the scale of supergranulation dependent on the resolution of the image we use rather than some intrinsic property of the pattern. The value of tile sizes of around 15 Mm obtained by us is due (in good part) to the particular resolution of the images we start with ($3''.2$ pixel^{-1} for the filtergrams). There is no a priori reason why supergranulation should prefer tessellation at this resolution. If we define supergranular scale as the mean tile size, then we do not have obvious grounds for excluding 10 Mm, the mean tile size derived from Dopplergrams, as the "true" supergranule size. Indeed, it follows from Figure 5 and has also been verified by us that sufficiently higher resolution K line filtergrams yield mean tile sizes much smaller than 10 Mm.

6.3. *Time Dependence of Tessellation*

The time dependence of the mean tessellation scale, as depicted in Figure 10, shows that the mean tile size gradually increases for about 24 hr, where an apparent leveling

off is seen. As noted, the tessellation scale derived from the Dopplergrams rises to over 16 Mm, while that from filtergrams rises to 23 Mm, the discrepancy being attributable to the difference in spatial resolution. In Figure 10, in the first 10 hr, both Dopplergram and filtergram mean tile sizes increase by about 4 Mm, which represents about 40% and 23% of the mean initial tile size of the respective data. All estimates of supergranular lifetime (as against size) are agreed on a value in excess of 20 hr (Leighton et al. 1962; Janssens 1970; Singh et al. 1994; Raju et al. 1998; Srikanth et al. 1999). Since Figure 10 implies that some of the tiles are averaged out within as few as 5 hr and thus have lifetimes less than this value, it is clear that these tiles cannot be identified with supergranules. We note that upon being averaged over supergranular lifetimes, the mean tile size in the K line approaches 23 Mm, quite close to the supergranular scales quoted by Singh & Bappu (1981) and Berilli et al. (1998). It would be interesting to check for this behavior in data of different resolutions.

6.4. *AC Scale and Tessellation Scale*

In contrast to tessellation scale, AC scale, as noted in connection with Figure 3, is fairly invariant under smoothing, and hence has approximately the same value in both Dopplergrams and filtergrams (about 30 Mm) for a range of resolution. The resolution indeterminacy of the tessellation method is absent in AC, which ensures a stable definition. However, AC size is rarely the true size when dealing with any realistic complicated structures, though it can be considered as a measure of size. Hagenaar et al. (1997) note that the tessellation scale is about 0.61 times the FWHM of the AC primary peak irrespective of the smoothing of the image. They conclude that the disparity between AC scale and tessellation scale is a result of AC responding preferentially to larger supergranules. In order to understand this feature, we determined the AC of the tessellated image. In such an image, the tile network pixels are set to a constant value, while tile interior pixels are set to another common lower constant value. This is equivalent to removing intensity information and retaining only topological/geometric information about the features. We found that AC of such a binary tessellated image gives a scale comparable to the tessellation scale, i.e., about one-half the usual AC scale. Thus, we attribute the lower AC scale to the removal of intensity information from the image. This removal is equivalent to boosting the relative contribution of lower intensity contrasts in the tessellated image. Conversely, the original image has an increased relative contribution of signals from structures with high intensity contrasts. Thus, the larger AC size in the original image is connected with the larger relative contribution from high-contrast features. Hence, AC picks its signal predominantly from high-contrast large features that possibly correspond to supergranules, whereas the basin-finding algorithm responds to all spatial intensity variations. We infer that while AC is underresponsive, a direct application of tessellation can be overresponsive to the network structures.

Since the AC size of supergranulation is typically 30–32 Mm (Leighton et al. 1962; Singh & Bappu 1981; Raju et al. 1998), the absence of well-defined AC signals at the 30 Mm scale can be taken as indicative of the absence of supergranules. We studied disk-center regions of (*p*-mode–filtered) Dopplergrams where, because of slow upflows and vanishing horizontal flows in the line of sight, weak supergranular signal is expected. We studied 14 over 70×70 Mm windows in the filtered *SOHO* Dopplergram disk centers. From this only two yielded AC scale greater than 25 Mm, indicative of a perceptible supergranular network. The tessellation scale derived from these two windows was found to be 7.55 ± 0.12. On the other hand, the mean tile scale for the remaining windows, which did not show evidence of supergranular signals, is found to be 7.63 ± 0.27. This shows that tessellation scale is independent of whether the supergranular signal (as manifested in the AC pattern) is weak or stronger in the given region. This corroborates our earlier conclusion, based on tessellation of phase-shifted self-averaged images, that the tessellation senses certain background spatial variations rather than solely supergranulation.

7. CONCLUSION

Morphological properties of supergranulation in Dopplergrams and the chromospheric network in Ca II K filtergrams were studied by a method of tessellation. It is shown that one can account for the difference between the Dopplergram and filtergram tessellations by taking into consideration the difference in resolution of the two image sets. This confirms that the morphological structure of the chromospheric network is similar to supergranulation as seen in Dopplergrams. The mean tessellation scale is found to increase when the images are spatially smoothed or temporally averaged, suggesting a depletion of small-scale tiles. The overall tendency for the distribution of the tiles is to broaden and become symmetrized as the image is spatially smoothed. However, there exists a degree of smoothing, which is characterized by a local peak in the skewness and kurtosis curves, at which the tessellation manifests the traditional scale of supergranules as well as their distributional properties. For an image at this resolution/smoothing, the tessellation is geometrically equivalent to supergranulation. The method proves to be a useful as well as intuitively appealing method to study patterns on the solar surface.

We thank P. H. Scherrer and the *SOHO* consortium for providing us with the MDI/SOI data. R. S. thanks V. Krishnakumar for useful discussions.

REFERENCES

Berilli, F., Ermolli, I., Florio, A., & Pietropaolo, E. 1999, A&A, 344, 965
Berilli, F., Florio, A., & Ermolli, I. 1998, Sol. Phys., 180, 29
Brune, R., & Wöhl, H. 1982, Sol. Phys., 75, 75
Duvall, T. L., Jr. 1980, Sol. Phys., 66, 213
Giovanelli, R. G. 1980, Sol. Phys., 67, 211
Hagenaar, H. J., Schrijver, C. J., & Title, A. M. 1997, ApJ, 481, 988
Hart, A. B. 1956, MNRAS, 116, 38
Janssens, T. J. 1970, Sol. Phys., 11, 222
Küveler, G. 1983, Sol. Phys., 88, 13
Leighton, R. B. 1964, ApJ, 140, 1547
Leighton, R. B., Noyes, R. W., & Simon, G. W. 1962, ApJ, 135, 474
Muller, R., & Roudier, Th. 1994, Sol. Phys., 152, 131
Münzer, H., Schröter, E. H., Wöhl, H., & Hanslmeier, A. 1989, Sol. Phys., 213, 431
Oda, N. 1984, Sol. Phys., 93, 243
Raghavan, N. 1983, Sol. Phys., 89, 35
Raju, K. P., Srikanth, R., & Singh, J. 1998, Sol. Phys., 178, 251
Rogers, E. H. 1970, Sol. Phys., 13, 57

Scherrer, P. H., et al. 1995, Sol. Phys., 162, 129
Schrijver, C. J., Hagenaar, H. J., & Title, A. M. 1997, ApJ, 475, 328
Simon, G., & Leighton, R. B. 1964, ApJ, 140, 1120
Singh, J., & Bappu, M. K. V. 1981, Sol. Phys., 71, 161
Singh, J., Nagabhushana, B. S., Babu, G. S. D., & Uddin, W. 1994, Sol. Phys., 153, 157
Srikanth, R., Raju, K. P., & Singh, J. 1999, Sol. Phys., 184, 267
Sýkora, J. 1970, Sol. Phys., 71, 161
Wang, H. 1988, Sol. Phys., 116, 1